Wall heat transfer effects on the hydro/thermal behaviour of Poiseuille flow in micro/nanochannels

Wall heat transfer effects on the hydro/thermal behaviour of Poiseuille flow in micro/nanochannels

Hassan Akhlaghi, Ehsan Roohi, Mojtaba Balaj, and S. Kokou Dadzie

Citation: Physics of Fluids (1994-present) **26**, 092002 (2014); doi: 10.1063/1.4894856
View online: http://dx.doi.org/10.1063/1.4894856
View Table of Contents: http://scitation.aip.org/content/aip/journal/pof2/26/9?ver=pdfcov
Published by the AIP Publishing

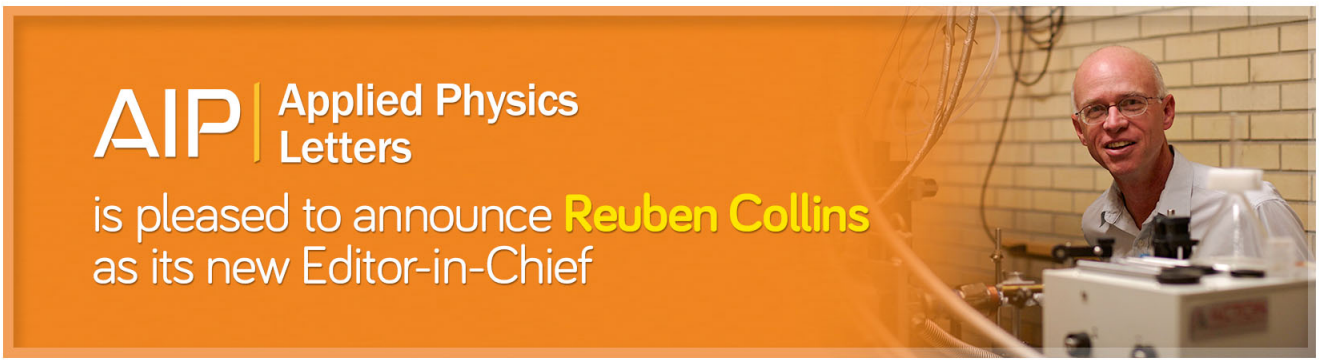

PHYSICS OF FLUIDS **26**, 092002 (2014)

Wall heat transfer effects on the hydro/thermal behaviour of Poiseuille flow in micro/nanochannels

Hassan Akhlaghi,[1] Ehsan Roohi,[1,a)] Mojtaba Balaj,[1] and S. Kokou Dadzie[2]
[1]*High Performance Computing (HPC) Laboratory, Department of Mechanical Engineering, Ferdowsi University of Mashhad, P.O. Box 91775-1111, Mashhad, Iran*
[2]*School of Engineering and Physical Sciences, Heriot-Watt University, Edinburgh, EH14 4AS, Scotland*

(Received 3 March 2014; accepted 25 August 2014; published online 8 September 2014)

We investigate effects of wall heat transfer on the structure of pressure driven flow in micro/nanochannels using the Direct Simulation Monte Carlo method. The effects of non-zero wall heat flux on the pressure distribution, velocity profiles, heat flow patterns, and the mass flow rate are reported. The simulation results show that cooling decreases slip at the wall and pressure along the channel. Cooling changes the heat flow direction along the channel while heating does not. At higher degree of rarefaction, the direction of the heat flow is mainly axial along the channel. An existence of cold-to-hot heat transfer process is demonstrated in the cooling wall case. Cooling can also create a heat singularity point in the domain. There is a critical Knudsen number about unity for which heating or cooling does not affect the mass flow rate through the channel. Below the critical Knudsen number, heating decreases and cooling increases the mass flow rate. Above it, heating increases and cooling decreases the mass flow rate. © *2014 AIP Publishing LLC*. [http://dx.doi.org/10.1063/1.4894856]

I. INTRODUCTION

Micromachining technology has become available to fabricate Micro- Nano-Electro-Mechanical Systems (MEMS/NEMS) such as plain channels which are the simplest and most common in micro-nanofluidic systems.[1] An important issue in the fabrication of micro- nano-mechanical devices is developing efficient techniques for thermal management of these devices. Hydrodynamic analysis of flows in micro-nano channels under thermal conditions is therefore very important for the development of MEMS/NEMS. As the Knudsen number, which is the ratio of the gas mean free path to the channel characteristic length, becomes large, the flow is analyzed using molecular-based methods instead of continuum-based approaches. Direct Simulation Monte Carlo (DSMC) is a useful method for non-equilibrium rarefied gas flows over a wide range of rarefaction.[2] In this method, the gas is modeled as a collection of moving particles which interact through collisions.

Along the extensive investigation of isothermal Poiseuille flow,[3,4] there are continuing attempts to understand heat transfer behaviour of micro-/nanochannel flows experimentally,[5,6] analytically, and numerically.[6–20] One of the first investigations of heat transfer for slip flows has been performed by Inman.[7] Inman studied a parallel plate channel with uniform wall temperature analytically. He considered the velocity slip and temperature jump and proposed an expression for the wall heat flux as a function of the rarefaction parameter. Kanki and Iuchi[8] presented a numerical solution of the Boltzmann equation with the Bhatnagar-Gross-Krook (BGK) model and showed that the effect of thermal creep on the velocity profile of Poiseuille flow is very large, especially at the Knudsen layer near the wall. They showed that the ratio of thermal creep to pressure driven effects approaches 0.5 as the gas density approaches zero and reduces to zero in the continuum flow limit.

[a)] Author to whom correspondence should be addressed. Electronic mail: e.roohi@ferdowsi.um.ac.ir. Tel.: +98 (513) 8805136. Fax: +98 (513) 8763304.

Ohwada *et al.*[9,10] investigated thermal transpiration flow of a rarefied gas between two parallel plates based on the linearized Boltzmann equation for hard sphere molecules. They obtained the velocity distribution of the gas molecules as well as the gas velocity and heat flow profiles, and mass flux for the whole range of Knudsen number. Hadjiconstantinou[11] used DSMC technique to investigate convective heat transfer in slip and transition regimes. He studied analytically the effect of shear work at the boundary with a constant wall heat flux. Myong *et al.*[12] investigated convective heat transfer in a microtube using a mathematical method extended from the classical Graetz problem. The effects of axial heat conduction were included in their study. They employed the Langmuir and conventional Maxwell model for surface slip and indicated that the Langmuir model shows always a decrease in heat transfer with increasing rarefaction. Weng and Chen[13] studied analytically natural convection gas flow through a long open-ended vertical parallel-plate microchannel with constant but not necessarily symmetrical wall heat fluxes. Results showed that thermal creep effect decreases the maximum gas temperature and the drag. Niazmand *et al.*[14] studied key flow parameters such as friction and heat transfer in an isoflux rectangular microchannel under heating. They showed that thermal creep reduces the friction coefficient and slightly enhances the heat transfer rate. Their study also showed that thermal creep effects become more pronounced at low Reynolds numbers. Taheri and Struchtrup[15] considered rarefied gas flow in a parallel-plate micro-channel under constant streamwise temperature gradient on the channel walls. They presented an analytical approach based on linearized and semi-linearized forms of the regularized 13-moment equations. They investigated velocity slip, temperature jump, and formation of Knudsen boundary layers. Ye *et al.*[16] investigated the thermal transpiration effect on hydrogen gas multiscale flow behaviours using DSMC-SPH coupling approach. They showed that when thermal transpiration is in the same direction as the driving pressure gradient, the velocity and the mass flow rate of the hydrogen flow increase. Ganguly *et al.*[17] discussed various rarefied gas dynamics aspects of freeze-drying including thermal creep and conduction, pressure, and concentration-gradient driven flows. They showed that the significance of the rarefied thermal creep varies greatly depending on temperature and pressure, and may be negligible at high pressure and low temperature gradient. Strapasson and Sharipov[18] studied sophisticated heat transfer phenomena due to temperature difference in He-Ar gas mixture through two parallel plates on the basis of the DSMC method with an implementation of a new "*ab initio*" molecular potential. They showed that the temperature distribution and heat flux between plates are weakly affected by molecular potential models. Contrary to previous works,[8–10,15] Akhlaghi *et al.*[19,20] considered a wide range of wall temperature gradients and investigated the variation of thermal mass flow rate. They showed that both wall heat flux and wall temperature gradient affect the mass flow rate in pressure driven flows.[19]

Despite these investigations, there is still a lack of results regarding the effect of non-zero wall heat flux on the flow structure and hydro/thermal behaviour of Poiseuille flow. Here we present a numerical investigation of a rarefied gas in a Poiseuille flow configuration submitted to gas-surface heat exchange with uniform wall temperature. Our study covers slip and transition regimes. Effects of heating and cooling on velocity profiles, pressure distributions, and heat flow patterns throughout the channel are presented. The trend of the normalized mass flow rate versus a newly introduced wall heat flux parameter is captured over a wide range of Knudsen number. Our DSMC simulation results on the mass flow rate and heat flow are new and there is no published article containing these results.

II. DIRECT SIMULATION MONTE CARLO MODELING

DSMC is considered as a particle method in which one particle represents a large bulk of real gas molecules. The primary principle of the DSMC method is decoupling linear motion and collision of the simulated particles. After fulfilling all movements, collisions between particles are simulated in each cell separately. In the present work, we extend a previous DSMC code developed by Roohi and co-workers for simulating micro-nano flows.[21–26] The variable hard sphere (VHS) model is applied as collision model in all simulations. As boundary conditions, we used the completely diffusive wall-reflection model where reflecting particles are not correlated with the incoming. The outgoing velocity of particles is assigned according to a Maxwellian distribution at the wall temperature;

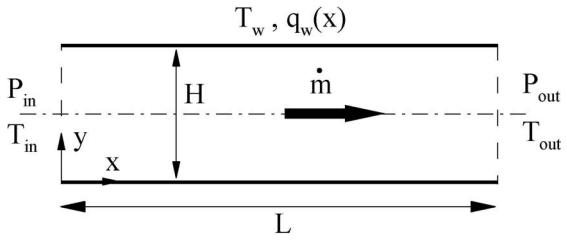

FIG. 1. Schematic of the channel and problem description.

therefore assuming a full thermal accommodation at the walls. Inlet and outlet pressure boundary conditions are implemented implicitly through correcting density and velocity values.[27,28] Details of the procedure and its verification are reported in a previous work.[26] The DSMC solver has been optimized with different features. Cell dimensions are chosen to be much less than one mean free path (λ).[29,30] This criterion is implemented based on the local mean free path in a cell. Each cell is subsequently divided into two subcells in each direction. Based on the VHS model, the mean free path of the gas is defined as a function of gas number density (n), molecular diameter (d), temperature (T), reference temperature (T_{ref}), and viscosity-temperature index (ω):[2]

$$\lambda = \frac{1}{\sqrt{2}\pi n d^2}\left(\frac{T}{T_{ref}}\right)^{\omega-0.5}. \quad (1)$$

Knudsen number is defined as the ratio of mean free path to the channel height, Kn = λ/H. The time step is taken to be a certain fraction of the mean collision time. Numbers of simulated particles are chosen such that there would be at least 20 particles in each cell.[31] Hadjiconstantinou[29] showed that DSMC error exhibits quadratic dependence on the time step, and that for time steps of the order of one mean free time the error is of the order of 5%. Our results are performed for time steps lees than 1/8 mean free path time for which the results are independent from the time step. Sampling of results starts as soon as the flow reaches steady state conditions. We have considered several items for checking the steady state condition: when the total number of simulation particles, intermolecular collision rate, and macroscopic properties (such as velocity, temperature, mass flow rate, etc.) no longer varies appreciably, i.e., less than 1%. Flow sampling continues in sufficiently large time step intervals. Nitrogen gas, $d = 4.65 \times 10^{-26}$ m, $T_{ref} = 273$ K, $\omega = 0.74$, $m = 4.17 \times 10^{-10}$ Kg, is employed as the working fluid for all simulations.

III. POISEUILLE FLOW UNDER HEATING/COOLING WALLS

We consider a pressure driven flow under non-zero wall heat transfer imposed by a wall-gas temperature difference ($T_w - T_{in}$). That is, we investigate a pressure driven flow under different uniform wall temperature conditions. Figure 1 depicts the channel geometry and the configuration under study. It is to be noted that this configuration is different from a thermal creep configuration where temperature gradients are imposed along the walls. The channel with inflow temperature (T_{in}) of 300 K, pressure ratio of 2, and aspect ratio of 6 are considered. Different degrees of wall heat transfer are achieved by varying values of T_w while the inflow temperature is kept constant. Different degrees of flow rarefaction are produced by adjusting the values of the inlet/outlet pressure ratio.

IV. HYDRODYNAMIC BEHAVIOUR

The effects of heating and cooling on the velocity profiles and centerline pressure distribution are shown in Figures 2 and 3 at initial and terminal sections of the channel. The average Knudsen numbers for the flows are 0.078 and 0.042 for heating and cooling cases, respectively. Negative values of q_w correspond to a heating wall where the wall temperature is greater than the inlet temperature. Figures 2(a) and 3(a) illustrate the wall heat flux distribution along the channel. As expected heat flux corresponding to the case $T_w = T_{in}$ is equal to zero along the channel. In the case of $T_w \neq T_{in}$,

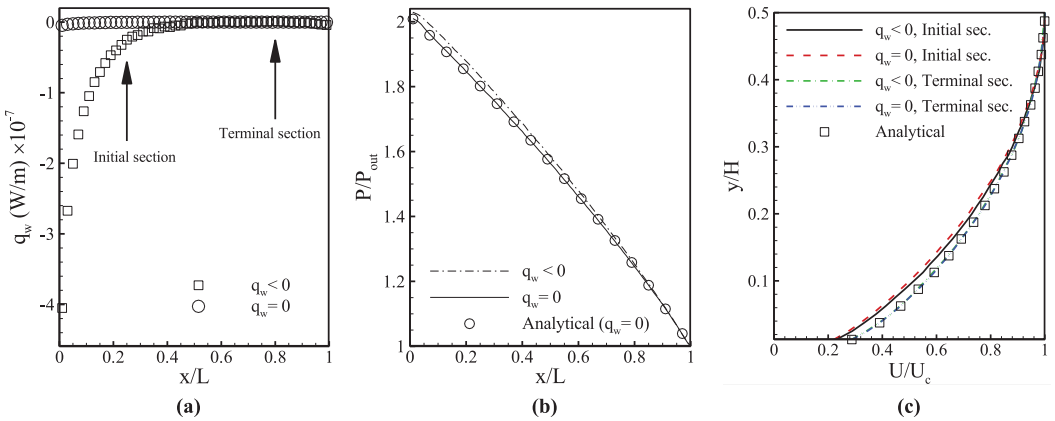

FIG. 2. Effects of heating on (a) wall heat flux, (b) pressure distribution, and (c) velocity profile.

the wall induces heating or cooling of the gas in the first half section of the channel. The magnitude of this heat flux decreases along the channel until it reaches zero. As flow moves along the channel, the average flow temperature increases until reaching the specified wall temperature where the heat transfer rate is zero leading to isothermal channel situation. In Figures 2(b) and 3(b), the simulation results for the pressure distribution are plotted alongside the isothermal analytical solution based on the second-order wall slip boundary conditions given by[32]

$$\left(\frac{P}{P_{out}}\right)^2 - 1 + 24C_1 Kn_{out}\left(\frac{P}{P_{out}} - 1\right) + 96C_2 Kn_{out}\log\left(\frac{P}{P_{out}}\right) + 2\mathrm{Re}\left(\frac{\mu^2(\kappa/m)T}{{P_{out}}^2 D_h^2}\right)$$
$$\left\{12C_1 Kn_{out}\left(\frac{P}{P_{out}} - 1\right)\right.$$
$$\left. + 24C_2 Kn_{out}\left[\left(\frac{P}{P_{out}}\right)^2 - 1\right] - \log\left(\frac{P}{P_{out}}\right)\right\} = -96\mathrm{Re}\left(\frac{\mu^2(\kappa/m)T}{{P_{out}}^2 D_h^2}\right) L\frac{X-1}{D_h}, \qquad (2)$$

where $X = x/L$ is the normalized streamwise location along the channel and $C_1 = 1.1466, C_2 = 0.9756$.[32] $D_h = 2H$ is the hydraulic diameter, κ is Boltzmann constant, μ is gas viscosity, and m is the molecular mass. According to Figures 2(b) and 3(b), the isothermal case results agree with the analytical solution as expected. The pressure distribution for the case $T_w \neq T_{in}$ deviates from the analytical solution in the first half section of the channel and agrees with it in the second half section where the local heat flux vanishes. We observe that heating increases the curvature, and vice

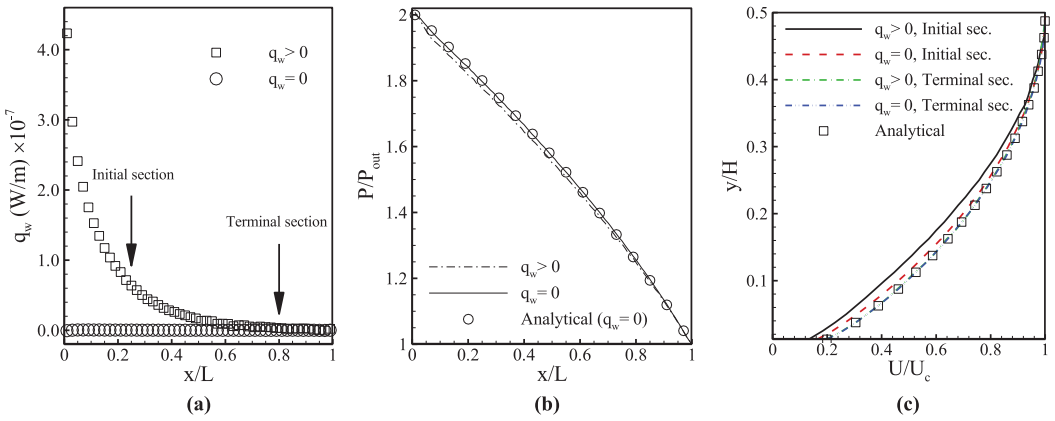

FIG. 3. Effects of cooling on (a) wall heat flux, (b) pressure distribution, and (c) velocity profile.

versa, in a manner that pressure distribution falls below the isothermal profile if the walls effectively cool down the flow field.[26] Figures 2(c) and 3(c) present dimensionless velocity profiles for the negative, zero, and positive values of the wall heat flux. The velocity is normalized by the centerline velocity, U_c. The velocity profiles are presented for a uniform Knudsen number in the channel. The initial and terminal sections correspond to $X = 0.3$ and $X = 0.8$, respectively. These profiles overlap at positions where the heat flux vanishes and differ in the non-zero wall heat flux regions (the entrance region of the channel). The analytical results[33] are presented for the terminal section. As the profiles are plotted for a constant Knudsen number, the change in velocity slip observed in the initial section of the channel is the result of local wall heat flux effects. According to Figures 2(c) and 3(c), heating increases the magnitude of velocity slip and cooling decreases it. This behaviour could be attributed to the pressure distribution along the channel. Pressure distribution for a cooling wall is lower than that of a heating wall, viz. Figures 2(b) and 3(b). Since the inlet pressure is the same for all cases, this pressure distribution leads to a larger pressure gradient ($\frac{dP}{dx} < 0$) for the hot wall. This large pressure gradient increases the velocity slip. Overall, the hydrodynamic behaviour of the gas flow through the channel is effectively affected by the local heat transfer. In other words, $\frac{U}{U_c} = f\left(Kn, \left.\frac{dP}{dx}\right|_{q\neq 0} - \left.\frac{dP}{dx}\right|_{q=0}\right)$.

Figure 4(a) shows variation of the average wall heat flux for different wall temperature values corresponding to heating and cooling cases over a wide range of inflow pressure magnitude covering the slip and high transition regimes. The average wall heat flux is defined by integration over the wall as

$$\overline{q_w} = \frac{1}{L}\int_{X=0}^{X=1} q_w(X)\,dX, \tag{3}$$

where q_w is the local wall heat flux rate, which is defined as the difference between the incident and reflected energy fluxes per unit time and per unit area of the wall:

$$q_w = \frac{\sum \varepsilon^i - \sum \varepsilon^r}{\Delta t.S}. \tag{4}$$

Figure 4(a) shows that the order of magnitude of the average wall heat flux differs for different inflow pressure levels. For $P_{in} = 6 \times 10^5$ Pa the average wall heat flux is of order 10^6, while for $P_{in} = 5 \times 10^3$ Pa the order of magnitude of the average wall heat flux is 10^4. The order of magnitude of the average wall heat flux decreases with increasing flow rarefaction. We define a reduced wall heat flux parameter (q^*) which remains in the same order over a wide range of flow rarefactions. It is defined as the average wall heat ($\overline{q_w}L$) divided by the inlet thermal energy ($\dot{m}c_pT_{in}$), where c_p is the specific heat capacity and $\dot{m}$ is the crossing mass flow rate. Figure 4(b) shows the variation of the reduced wall heat flux for different wall temperature values corresponding to heating and cooling conditions. According to Figure 4(b), absolute values of q^* lie between zero and unity for different levels of the flow rarefaction and different heating and cooling conditions. It is therefore an appropriate parameter to evaluate effects of the wall heat flux.

V. HEAT FLOW

Thermal patterns and heat lines within the channel are presented in this section for the non-zero wall heat flux cases. Heat flux in the domain is calculated using the following kinetic theory relations:[2]

$$q_x = \frac{1}{2}\rho\overline{c'^2u'} + n\overline{\varepsilon_{\text{int}}u'}, \tag{5}$$

$$q_y = \frac{1}{2}\rho\overline{c'^2v'} + n\overline{\varepsilon_{\text{int}}v'}, \tag{6}$$

where c' is the peculiar velocity vector and ε_{int} is the internal energy of a single particle. n is the number density, ρ is the mass density, and u', v' are components of c'. Similar to wall heat flux, we

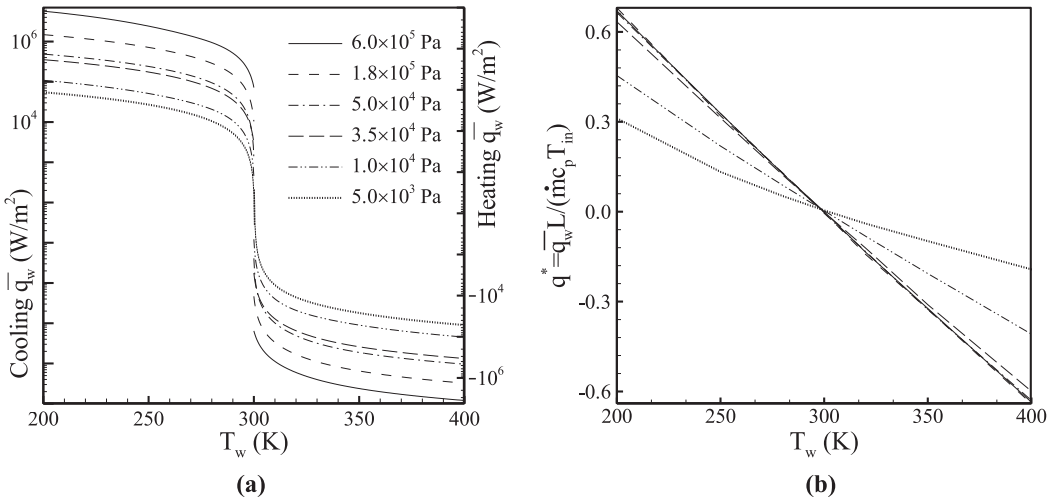

FIG. 4. Variation of (a) averaged wall heat flux and (b) reduced wall heat flux as a function of wall temperature for different levels of inflow pressure.

normalize the heat flux in the domain as follows:

$$q_x^* = \frac{q_x H}{\dot{m} c_p T_{in}}, \tag{7}$$

$$q_y^* = \frac{q_y L}{\dot{m} c_p T_{in}}. \tag{8}$$

Profiles of the reduced tangential and normal heat flux are shown in Figures 5 and 6 at two streamwise locations, i.e., $X = 0.2$, 0.8. These two locations have, respectively, non-zero and zero wall heat flux conditions. The heat lines overlaid on the temperature contours are shown in Figure 7. The results are obtained for different levels of inflow pressure of 6×10^5 Pa, 5×10^4 Pa, and 5×10^3 Pa corresponding to slip, early transition, and high transition regimes. Both upper and lower walls have the same temperature: 200 K and 400 K for cooling and heating conditions, respectively. Isothermal condition ($T_w = 300$ K) is associated with inflow pressures of 6×10^5 Pa,

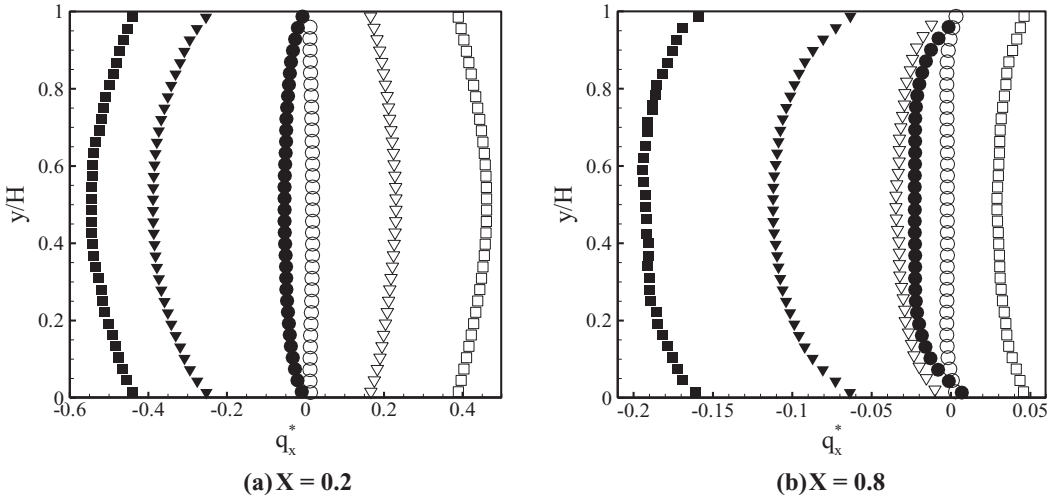

FIG. 5. Reduced tangential heat flux profile for heating (filled symbols) and cooling (blanked symbols) conditions at different sections of channel and inflow pressures of 6×10^5 Pa (circles), 5×10^4 Pa (triangles), and 5×10^3 Pa (squares).

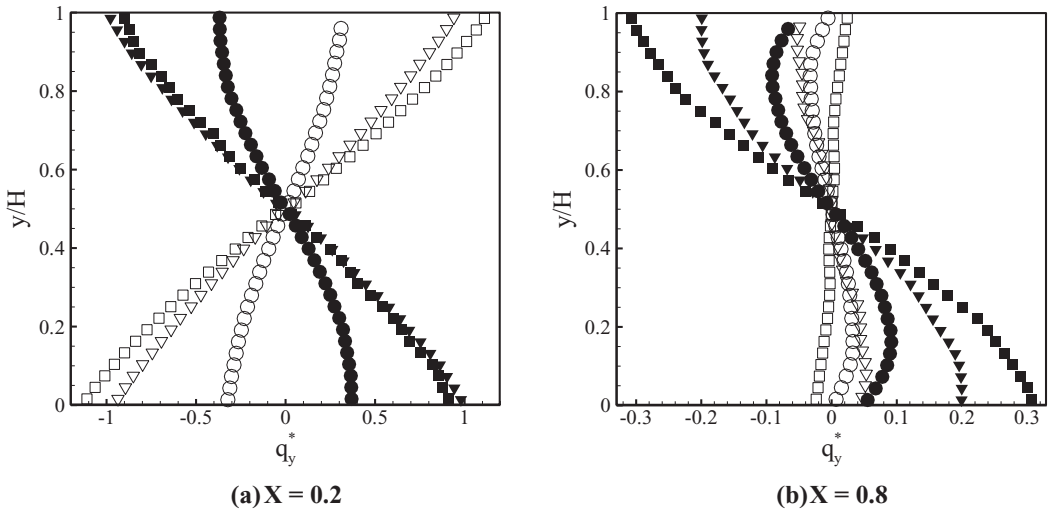

FIG. 6. Reduced normal heat flux profile for heating (filled symbols) and cooling (blanked symbols) conditions at different sections of channel and inflow pressures of 6×10^5 Pa (circles), 5×10^4 Pa (triangles), and 5×10^3 Pa (squares).

5×10^4 Pa, and 5×10^3 Pa, (or $Kn_{avg} = 0.06$, 0.74, and 7.3, respectively) i.e., slip, early transition, and high transition flow regimes. It is observed that the magnitude of both the reduced tangential and normal heat flux increases with an increase in Knudsen number. The tangential heat flux profiles also show several interesting trends. First, the tangential heat flux yields a profile that is much flatter across the channel centerline in the slip regime (circles in Figure 5). This behaviour, however, reduces with an increase in the flow rarefaction as the profile follows a parabolic shape in the transition regime (triangles and squares in Figure 5). More interestingly, in Figure 6, the reduced normal heat flux reveals a sinusoidal behaviour for all Knudsen numbers. This figure also shows that the normal heat flux is maximum in near-wall regions while it vanishes at the center of the channel. This means that the net heat flow direction along the channel centerline is determined only by the

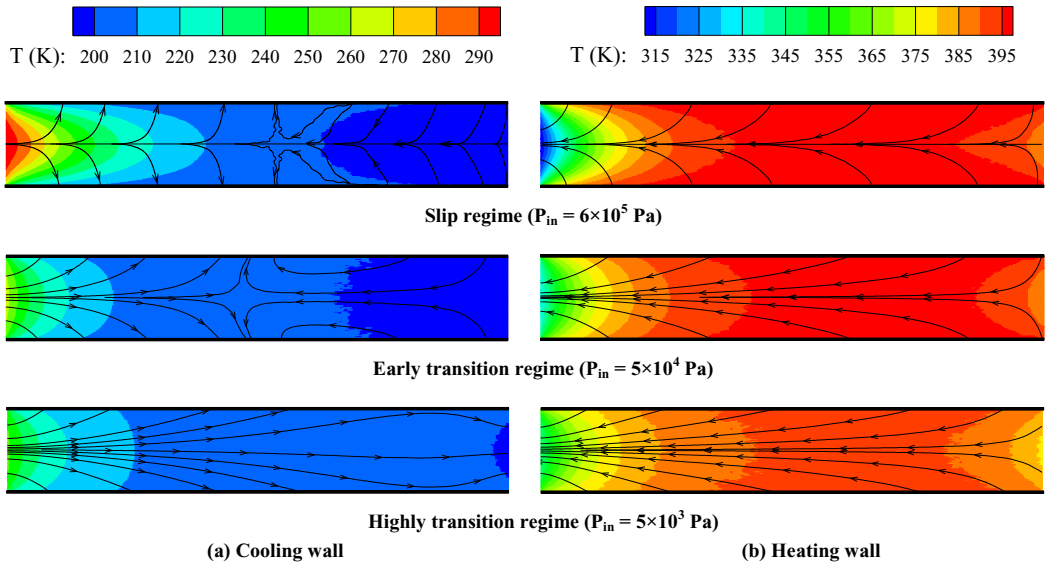

FIG. 7. Heat lines overlaid on the temperature contour for cooling ($T_w = 200$ K) and heating ($T_w = 400$ K) walls at different flow regimes.

tangential heat flux (viz. Figure 7), whereas the normal heat flux plays an important role near the walls as it changes the net heat flow direction in these regions considerably.

At $X = 0.2$ the reduced normal heat flux is much higher for the transition regime (viz. triangles and squares with circles in Figure 6(b)). Along the center of the channel where the normal heat flux is equal to zero, the net heat flow is always parallel to the x direction (Figure 7). The predicted tangential heat flux at $X = 0.2$ indicates that for cold walls ($T_w < T_{in}$) the heat flux is positive and for hot walls ($T_w > T_{in}$) it is negative. This means that the heat flow along the centerline is in the direction opposite to the mass flux for heating walls while it is in the direction of mass flux for cooling walls, see Figure 7. The computed tangential heat flux at $X = 0.8$ shows that the heat flux at that location is always in the direction opposite to the mass flux except in the case of cooling condition at high transition regime where $q_x > 0$. Therefore, for this latter case the centerline heat flux is in the direction of the mass flow along the entire channel (Figure 7). The phenomenon of thermal creep arises due to the tangential heat flux along the channel with the gas moving from the cold region towards the hot region. The cold walls have positive thermal creep effects and the hot walls lead to a negative thermal creep. In Sec. VI we discuss how the positive thermal creep of the cold walls increases the mass flow rate through the channel.

In micro-nanochannel flows, viscous heating, expansion cooling, and non-equilibrium effects are the main parameters that determine the temperature field. Viscous dissipation always acts as a heat source and is dominant where the shear stresses are strong, i.e., near wall regions. From Figure 7 we observe that there is a significant drop in temperature at the outlet, particularly for the cases of heating walls. This may be attributed to the expansion cooling near the outlet. Non-equilibrium effects are driven by the gas-surface temperature difference. An interesting heat flow pattern is seen in the axial direction for the cooling wall condition. Heat flow along the channel-centerline is in the direction of the mass flow in the first half of the channel. In the second half, it is instead in the opposite direction, except in the case of higher rarefactions. This demonstrates an existence of cold-to-hot heat transfer process in the cooling wall cases. However, this phenomenon does not appear in the case of heating walls, where the heat flow is unidirectional and always in the opposite direction of mass flow rate. This cold-to-hot heat transfer process is specific to rarefied gas confined in micro- nano- devices and cannot be predicted using the Navier-Stokes-Fourier set of equations.[25,34]

VI. MASS FLOW RATE

In this section we present effects of varying wall temperature on the mass flow rate through the channel. Figure 8 illustrates the variation of the channel mass flow rate as a function of the wall temperature for a range of flow rarefaction covering both slip and transition regimes.

Figure 8 demonstrates that the mass flow rate decreases as the wall temperature increases until an inflow pressure of 3.5×10^4 Pa, which corresponds to an average Knudsen number of about unity. It means that cooling leads to an increase in the mass flow rate and the heating causes a reduction instead. This behaviour changes in the higher transition flow regime. For inflow pressures of 10^4 Pa and 5×10^3 Pa the mass flow rate increases as the wall temperature increases. For the case of an inflow pressure of 3.5×10^4 Pa, the mass flow rate remains approximately unchanged with heating and cooling processes. We also see that the rate of change in mass flow rate for the cooling walls is greater than that of the heating walls in both slip and transition regimes. The mass flow rate varies nonlinearly with the wall heat flux.

To evaluate this nonlinear behaviour of the mass flow rate versus heating/cooling processes, we consider a non-dimensional form of the mass flow rate ($\dot{m}_n$) by its isothermal value ($T_w = 300$ K). We analyze the variation of this non-dimensional mass flow rate as a function of the non-dimensional wall heat flux. Figure 9 shows the normalized mass flow rate versus the reduced wall heat flux for different levels of flow rarefaction. Heating and cooling processes affect much more the mass flow rate in the slip regime (inflow pressures of 1.8×10^5 Pa and 6×10^5 Pa). For the flow with Knudsen number of unity (inflow pressures of 3.5×10^4), the mass flow rate is not affected by heating or cooling. The effect of heating and cooling in the higher transition flow regime is almost independent of the Knudsen number (comparing cases with inflow pressure of 5.0×10^3 Pa and 1.0×10^4 Pa).

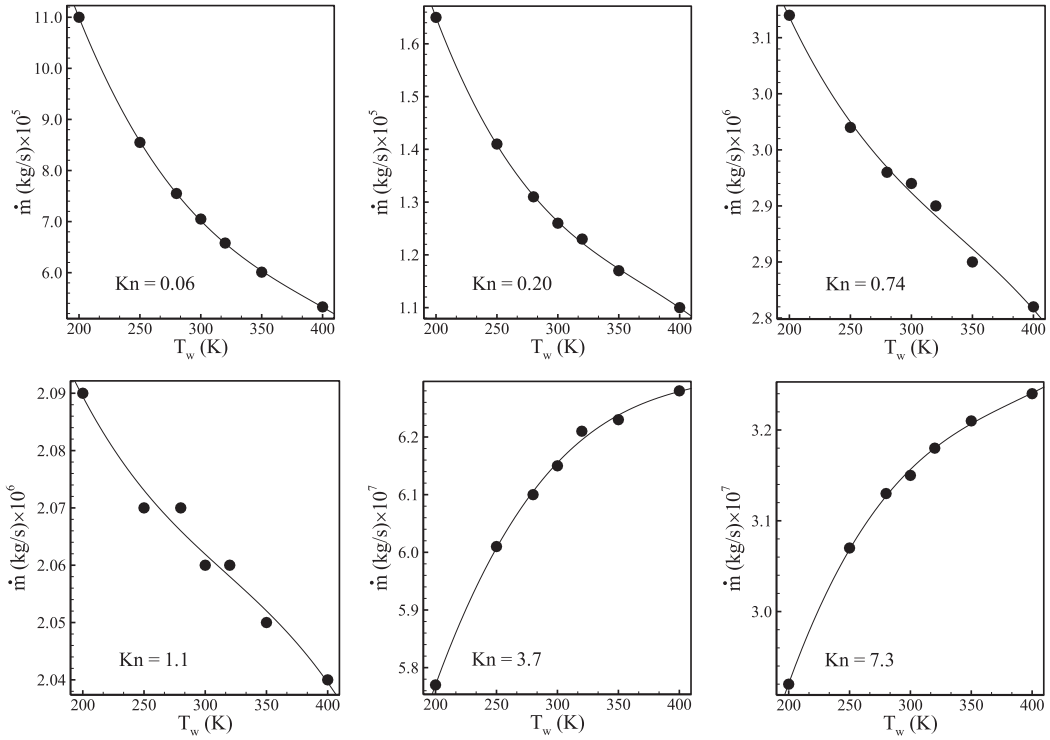

FIG. 8. Mass flow rate variation as function of wall temperature and wall heat flux over a wide range of Knudsen numbers.

Gas viscosity varies with temperature according to $\mu = \mu_{ref}(T/T_{ref})^{\omega}$. Therefore, heating (/cooling) decreases (/increases) the mass flow rate via increasing (/decreasing) viscosity and decreasing (/increasing) density. As Knudsen number increases, thermal creep effects become stronger. Heating produces streamwise temperature gradient in the Knudsen layer and leads to an increasing mass flow rate.[19,20] Thermal creep affects the mass flow rate in a reverse manner with respect to viscosity

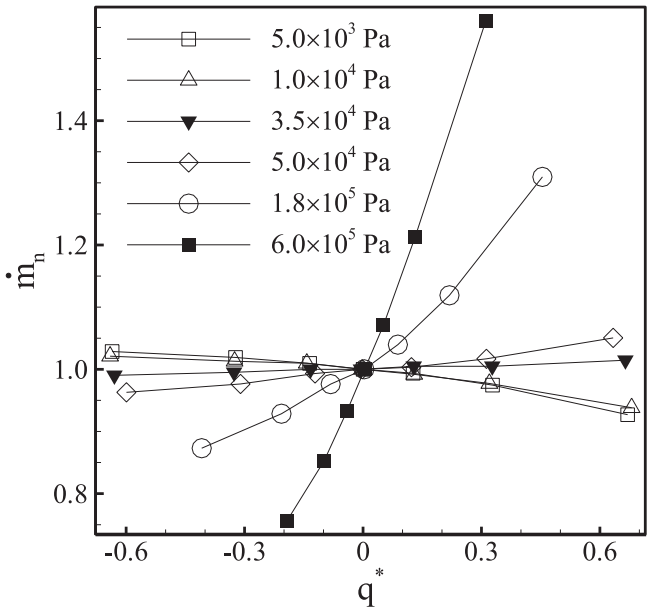

FIG. 9. Normalized mass flow rate as a function of reduced wall heat flux for different flow rarefactions.

and density variation. For Knudsen numbers greater than unity, the Knudsen layer covers the entire channel. From Figure 9, for the higher transition flow regime, thermal creep effects are dominant and heating increases mass flow rate despite the negative effects of decreasing density and increasing viscosity. For Knudsen numbers about unity, the thermal creep effects are in balance with density and viscosity variations, and the mass flow rate remains constant with heating/cooling wall heat fluxes. In slip and early transition regimes, viscosity and density changes are dominant with weak thermal creep effects and heating (/cooling) decreases (/increases) the mass flow rate.

VII. CONCLUSION

We presented a DSMC investigation of a rarefied Poiseuille flow under heating and cooling wall heat fluxes over a wide range of flow rarefactions from slip to high transition regime. We considered effects of heating and cooling on the velocity profiles, heat flow patterns, and the mass flow rate. It is detected that heating increases and cooling decreases the slip at the walls. Heating also increases and cooling decreases the pressure compared with the isothermal pressure profile. The results showed that the heating and cooling wall heat fluxes significantly affect the heat flow pattern in the domain. A cold-to-hot heat transfer process occurs in the cooling wall case at slip and early transition flow regimes. In these cases, there is a heat singularity point in the domain. Also, in the high transition regime, the streamwise heat flow is dominant compared to the lateral one in the domain. A critical Knudsen number about unity was detected for which heating or cooling does not affect the mass flow rate through the channel. Below that, heating decreases and cooling increases the mass flow rate and above that, heating increases and cooling decreases the mass flow rate.

ACKNOWLEDGMENTS

The authors would like to acknowledge the financial supports provided by Ferdowsi University of Mashhad under Grant No. 28152.

[1] C. M. Ho and Y. C. Tai, "Micro-electro-mechanical-system (MEMS) and fluid flows," Annu. Rev. Fluid Mech. **30**, 579 (1998).
[2] G. A. Bird, *Molecular Gas Dynamics and the Direct Simulation of Gas Flows* (Clarendon, Oxford, UK, 1994).
[3] E. J. Arlemark, S. K. Dadzie, and J. M. Reese, "An extension to the Navier-Stokes equations by considering molecular collisions with boundaries," J. Heat Transfer **132**, 041006 (2010).
[4] S. K. Dadzie and H. Brenner, "Predicting enhanced mass flow rates in micro gas channels using non-kinetic models," Phys. Rev. E **86**, 036318 (2012).
[5] M. Miyamoto, W. Shi, Y. Katoh, and J. Kurima, "Choked flow and heat transfer of low density gas in a narrow parallel-plate channel with uniformly heating walls," Int. J. Heat Mass Transfer **46**, 2685 (2003).
[6] S. Colin, P. Lalonde, and R. Caen, "Validation of a second-order slip flow model in rectangular microchannels," Heat Transfer Eng. **25**, 23 (2004).
[7] R. Inman, "Laminar slip flow heat transfer in a parallel plate channel or a round tube with uniform wall heating," NASA Technical Note D-2393, 1964.
[8] T. Kanki and S. Iuchi, "Poiseuille fllow and thermal creep of a rarefied gas between parallel plates," Phys. Fluids **16**, 594 (1973).
[9] T. Ohwada, Y. Sone, and K. Aoki, "Numerical analysis of the shear and thermal creep flows of a rarefied gas over a plane wall on the basis of the linearized Boltzmann equation for hard-sphere molecules," Phys. Fluids A **1**, 1588 (1989).
[10] T. Ohwada, Y. Sone, and K. Aoki, "Numerical analysis of the Poiseuille and thermal transpiration flows between two parallel plates on the basis of the Boltzmann equation for hard-sphere molecules," Phys. Fluids A **1**, 2042 (1989).
[11] N. G. Hadjiconstantinou, "Dissipation in small scale gaseous flows," J. Heat Transfer **125**, 944 (2003).
[12] R. S. Myong, D. A. Lockerby, and J. M. Reese, "The effect of gaseous slip on microscale heat transfer: An extended Graetz problem," Int. J. Heat Mass Transfer **49**, 2502 (2006).
[13] H. C. Weng and C. Chen, "On the importance of thermal creep in natural convective gas microflow with wall heat fluxes," J. Phys. D: Appl. Phys. **41**, 115501 (2008).
[14] H. Niazmand, A. Amiri Jaghargh, and M. Renksizbulut, "Slip-flow and heat transfer in isoflux rectangular microchannels with thermal creep effects," J. Appl. Fluid Mech. **3**, 33 (2010).
[15] P. Taheri and H. Struchtrup, "Rarefaction effects in thermally-driven microflows," Physica A **389**, 3069 (2010).
[16] J. Ye, J. Yang, J. Zheng, X. Ding, I. Wong, W. Li, and C. Chen, "Thermal transpiration effect on the mass transfer and flow behaviors of the pressure-driven hydrogen gas flow," Int. J. Hydrogen Energy **37**, 12474 (2012).
[17] A. Ganguly, S. L. Nail, and A. A. Alexeenko, "Rarefied gas dynamics aspects of pharmaceutical freeze-drying," Vacuum **86**, 1739 (2012).

[18] J. L. Strapasson and F. Sharipov, "Ab initio simulation of heat transfer through a mixture of rarefied gases," Int. J. Heat Mass Transfer **71**, 91 (2014).
[19] H. Akhlaghi and E. Roohi, "Mass flow rate prediction of pressure–temperature-driven gas flows through micro/nanoscale channels," Continuum Mech. Thermodyn. **26**, 67 (2014).
[20] H. Akhlaghi, M. Balaj, and E. Roohi, "Hydrodynamic behaviour of micro/nanoscale Poiseuille flow under thermal creep condition," Appl. Phys. Lett. **103**, 073108 (2013).
[21] A. Amiri-Jaghargh, E. Roohi, H. Niazmand, and S. Stefanov, "DSMC simulation of low Knudsen micro/nano flows using small number of particles per cells," J. Heat Transfer **135**, 101008 (2013).
[22] J. A. Esfahani, O. Ejtehadi, and E. Roohi, "Second law analysis of micro/nano Couette flow using DSMC," Int. J. Exergy **13**, 320 (2013).
[23] A. Amiri-Jaghargh, E. Roohi, S. Stefanov, H. Nami, and H. Niazmand, "DSMC simulation of micro/nano flows using SBT-TAS technique," Comput. Fluids **102**, 266 (2014).
[24] M. Balaj, E. Roohi, H. Akhlaghi, and R. S. Myong, "Investigation of convective heat transfer through constant wall heat flux micro/nano channels using DSMC," Int. J. Heat Mass Transfer **71**, 633 (2014).
[25] A. Mohammadzadeh, E. Roohi, H. Niazmand, S. K. Stefanov, and R. S. Myong, "Detailed investigation of thermal and hydrodynamic behaviour in micro/nano cavity using DSMC," Phys. Rev. E **85**, 056305 (2012).
[26] H. Akhlaghi, E. Roohi, and S. Stefanov, "A new iterative wall heat flux specifying technique in DSMC for heating/cooling simulations of MEMS/NEMS," Int. J. Therm. Sci. **59**, 111 (2012).
[27] W. Liou and Y. Fang, "Implicit boundary conditions for direct simulation Monte Carlo method in MEMS flow predictions," Comput. Model. Eng. Sci. **1**, 119 (2000).
[28] M. Wang and Z. Li, "Simulations for gas flows in microgeometries using the direct simulation Monte Carlo method," Int. J. Heat Fluid Flow **25**, 975 (2004).
[29] N. G. Hadjiconstantinou, "Analysis of discretization in the direct simulation Monte Carlo," Phys. Fluids **12**, 2634 (2000).
[30] Z. X. Sun, Z. Tang, Y. L. He, and W. Q. Tao, "Proper cell dimension and number of particles per cell for DSMC," Comput. Fluids **50**, 1 (2011).
[31] C. Shu, X. H. Mao, and Y. T. Chew, "Particle number per cell and scaling factor effect on accuracy of DSMC simulation of micro flows," Int. J. Numer. Methods Heat Fluid Flow **15**, 827 (2005).
[32] N. Dongari, A. Agrawal, and A. Agrawal, "Analytical solution of gaseous slip flow in long microchannels," Int. J. Heat Mass Transfer **50**, 3411 (2007).
[33] A. Beskok and G. E. Karniadakis, "A model for flows in channels, pipes, and ducts at micro and nano scales," Microscale Thermophys. Eng. **3**, 43 (1999).
[34] B. John, X. J. Gu, and D. R. Emerson, "Nonequilibrium gaseous heat transfer in pressure-driven plane Poiseuille flow," Phys. Rev. E **88**, 013018 (2013).